Nature Environment and Pollution Technology
An International Quarterly Scientific Journal

p-ISSN: 0972-6268
(Print copies up to 2016)
e-ISSN: 2395-3454

Vol. 23 | No. 4 | pp. 2291-2303 | 2024

Original Research Paper

https://doi.org/10.46488/NEPT.2024.v23i04.033

Open Access Journal

Investigations on Photodegradation and Antibacterial Activity of Mixed Oxide Nanocrystalline Materials

P. P. Shinde[1], R. J. Sayyad[1], S. S. Shukla[1], S. A. Waghmode[2] and S. R. Gadale[1†]

[1]Yashwantrao Mohite College of Art, Science and Commerce, Bharati Vidyapeeth Deemed to be University, Pune, India
[2]MES, Garware College, Pune, India
†Corresponding author: S. R. Gadale; dagade@rediffmail.com

Nat. Env. & Poll. Tech.
Website: www.neptjournal.com

Received: 20-02-2024
Revised: 26-03-2024
Accepted: 29-04-2024

Key Words:
Mixed oxide
Cobalt doped molybdenum
Catalytic activity
Methyl orange
Methylene blue
Microbial analysis

ABSTRACT

In this study, we synthesized cobalt-doped molybdenum supported on silica (Co/MS) nanocomposites with varying concentrations of cobalt (1, 5, 10, 15, and 20 wt%) using the sol-gel method. We investigated their physico-chemical properties, photocatalytic activity, and antimicrobial efficacy. The synthesized nanocomposites were characterized using a range of techniques, including X-ray powder diffraction (XRD) to determine crystal structure, UV-vis spectroscopy for optical properties, Fourier transform infrared spectroscopy (FT-IR) for functional group analysis, and scanning electron microscopy coupled with energy-dispersive X-ray microanalysis (SEM-EDX) for morphological and elemental composition analysis. The photocatalytic performance of these catalysts was assessed by their ability to degrade organic dyes, specifically methyl orange and methylene blue, under visible light irradiation. Our results demonstrated that the photocatalytic efficiency increased with higher cobalt content, with the 20 wt% Co/MS nanocomposite showing the highest degradation rates. Additionally, we evaluated the antibacterial activity of the nanocomposites against a range of microorganisms, including Gram-positive and Gram-negative bacteria, as well as fungal species. The 20 wt% Co/MS nanocomposite exhibited superior antimicrobial activity compared to the other samples, indicating its potential for applications in environmental remediation and antimicrobial treatments.

INTRODUCTION

The world population is growing faster in this era. Hence, to satisfy the demands of the people, newer industries and medical laboratories are being established all over the world. When such places release their wastewater into freshwater systems without first treating it, it adversely affects the natural ecosystem, including aquatic life (Gita et al. 2017, Kant 2015). These industries' harmful byproducts contain a variety of dangerous dyes that represent a significant danger to aquatic life and ecosystems (Manzoor & Sharma 2020, Lellis et al. 2019) Worldwide, many factories are responsible for water and air pollution, which can be seen from the disturbed ecosystem and climate (Zhang et al. 2010). It is clear that reducing population is significantly more challenging than improving industrial plant safety and pollution control (Weber & Sciubba 2019). Rather than employing traditional water purification techniques, one should discover more practical and environmentally beneficial wastewater treatment methods (Pandit et al. 2015). These techniques utilize physical, chemical, and biological techniques, including membrane separation, ozonation, adsorption, biological digestion, and clay minerals (Buonomenna 2013, Putatunda et al. 2015). While each of these methods has advantages and disadvantages, the scientific community is searching for more efficient water purification techniques. (Bian et al. 2015, Kou et al. 2014). The textile sector is a big contributor to water pollution because it needs vibrant dyes and pigments to produce garments more effectively (Isik & Sponza 2005). Methyl red, methyl orange, methylene blue, rhodamine 6B, rose Bengal, congo red, and crystal violet have been used consistently in the textile industry up until now. Nearly all of the dyes mentioned above have been thoroughly examined for both their benefits and drawbacks; several of them are poisonous to people when they come into touch with them (Lan et al. 2014). Finding an alternative or alternative procedure for the treatment of dirty waste water is required because this is a very important problem. Recently, the environmental remediation process has successfully used the heterogeneous photocatalysis approach (Fang et al. 2013). Typically, semiconductor oxides are used as a catalyst in photocatalysis techniques in the presence of light. The electron from the semiconductor's valence band (VB) reaches the conduction band (CB) in the presence of light of the right wavelength, producing electron-hole pairs (Mills et al. 1993). Superoxide anion radicals are produced when the CB electron reacts with

oxygen molecules that were adsorbed on the surface, while OH radicals are produced when the VB hole reacts with water molecules. These freshly formed superoxide anions and OH radicals have enhanced reducing and oxidizing capacities and, therefore, can reduce or oxidize a wide variety of substances (Lu et al. 2013). Herein, we have prepared the Co-doped MoO_3/SiO_2 nanocomposite with different concentrations using the sol-gel reaction technique, calcined at temperatures of 500°C, and studied its photocatalytic activity towards methyl orange degradation.

Global public health is seriously threatened by the spread of infectious illnesses, especially as antibiotic-resistant bacterial species proliferate. Bacterial species, both Gram-positive and Gram-negative, are generally regarded as major hazards to public health. Over the years, Antibiotics have been used to treat infections caused by environments observed in both hospitals and the community (Komolafe 2003, Hawkey 2008). New antibacterial medications are likely to be developed as a result of recent developments in nanobiotechnology, specifically the capacity to generate metal oxide nanoparticles of a particular size and shape. The primary factor affecting the functional activity of the nanomaterials is their particle size. Because of their exceptional physical, chemical, and biological qualities, nanomaterials have drawn a lot of interest from a variety of industries, and medicine is no exception.

Additionally, it has been noted that nanoparticles with lower particle sizes exhibit good antibacterial action (Jones et al. 2008). There is very little information available on the antibacterial characteristics of metal oxide nanoparticles compared to published publications on their physical and chemical properties. Realizing the potential antimicrobial applications of metal oxide nanoparticles and taking these characteristics into account, we employed Co-doped MoO_3/SiO_2 nanocomposite at varying concentrations to study their antifungal and antibacterial properties against Gram-positive (S. aureus) bacteria and Gram-negative (*Pseudomonas aeruginosa* and *E. coli*). Also, two fungal strains were used, i.e., *Candida albicans* and *Aspergillus niger.*

MATERIALS AND METHODS

Materials

The chemicals used for the preparation of nanocatalysts were analytical grade (A.R.) All the reagents viz. Ammonium heptamolybdate, tetra ethyl orthosilicate (Chemplast, Chennai, CAS register no. 18945-71-7), isopropyl alcohol (IPA), and Cobalt nitrate were AR grade (99.8%) and acquired from S.D. Fine, Thomas Baker, LOBA, and Merck Chemicals India. Distilled water was used as a solvent as well as for catalyst synthesis.

Methods

Using a Rigaku Miniflex G-600 diffractometer set to scan at a rate of 10°/min, an X-ray diffraction (XRD) study was conducted at room temperature to record the pattern in the 2θ range of 10-80. Measurements using a scanning electron microscope (SEM) were made using a Nova Nano SEM (NPEP303). Using a 15 k beam energy, SEM-associated energy-dispersed X-ray microanalysis (EDX) was used to examine the elemental compositions. Thermo Nicolet iS5 IR device was used to perform Fourier Transfer InfraRed spectroscopy at room temperature with KBr pellets at a resolution of 4 cm^{-1} in the 4000-400 cm^{-1} range and 32 scans. Using a Shimadzu UV-3600 model UV-Vis-NIR spectrophotometer, the optical investigation was conducted between 200 and 800 nm in wavelength. The absorption spectra of UV-visible were noted.

Synthesis of $Co/Mo/SiO_2$ Catalysts

Co-doped on Mo/SiO_2, nanomaterial was prepared by simple sol-gel method to obtain the material with high surface area as well as for uniform distribution of Co/Mo on silica support tetraethyl orthosilicate was used as a silica source. In this work, nanocatalyst was synthesized with different wt.% cobalt oxide concentrations (1, 5, 10, 15, and 20 wt. %). A suitable amount of cobalt nitrate was dissolved in distilled water for the synthesis of Co-doped on a MoO_3/SiO_2 nanomaterial. This cobalt nitrate aqueous solution was added dropwise to a mixture of AHM and TEOS solution. After that, the sol formed was stirred for 5 h at room temperature. The resultant bluish gel was further dried overnight at room temperature. The gel was kept in an oven at 100°C for 12 h while xerogel powder was obtained, which was calcined at 500°C temperatures for 4 h.

RESULTS AND DISCUSSION

Fourier Transfer Infrared Spectroscopy (FT-IR)

The bending and stretching vibrations of the functional groups present in the samples were obtained by FTIR studies. Fig. 1 displays the FTIR spectra of a Co-doped Mo/SiO_2 (Co/MS) nanomaterial that was calcined at 500°C for 4 h. A moderate absorption band, produced by the O-H bond's bending vibration, appeared at 1631.40 cm^{-1}. These absorption bands are a result of hydroxyl and water absorbed on the sample surface (Fig. 1). A strong absorption band present at approximately 1072.54 cm^{-1} was due to the vibration of the chemical bond of Si-O-Si which confirms

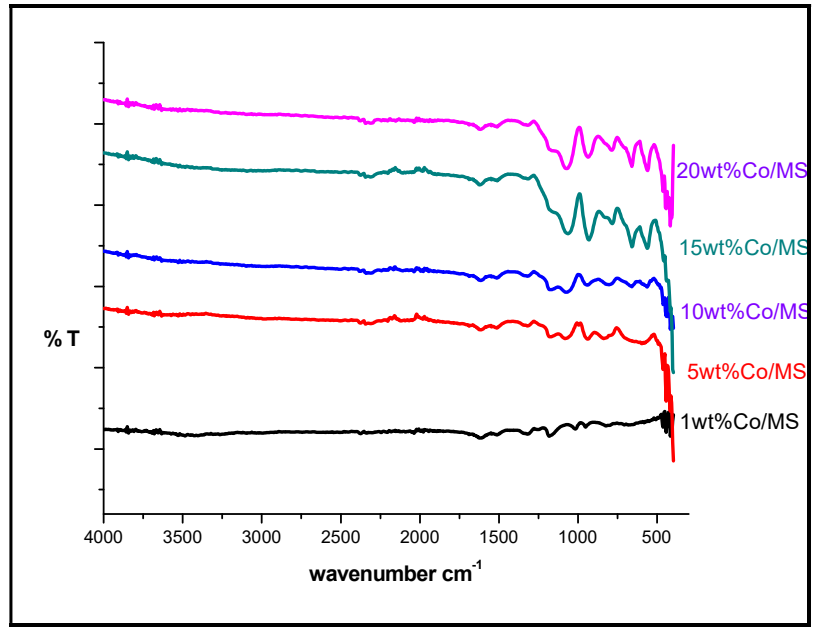

Fig. 1: FT-IR Spectra of 1-20 wt % Co/MS nanocatalysts.

the interaction between molybdenum and supported matrix. Additionally, the new peaks for the 1, 5, 10, 15, and 20 wt % Co-doped MS are located at around 556.41 cm^{-1}, and these correspond to the Co-O stretching mode in the tetrahedral site and octahedral environment (Rahman et al. 2021). The peaks at 778.32 and 809.55 cm^{-1} can be assigned to vMo-O vibrations. The peaks at 936.11 cm1 were attributed to the Mo-O-Mo of Mo^{6+} (Chiang & Yeh 2014, Dong & Dunn 1998, Muhammad et al. 2021).

Uv-Visible Spectroscopy

Understanding the electronic structure of the material for the optical study, especially the band gap study, was done with the analysis of the UV–Vis absorption spectrum. Fig. 2(a) illustrates the UV-visible absorbance spectrum of synthesized Co/MS (1-20wt%), which was measured in diffuse reflectance mode between 200 and 800 nm. The UV-visible absorbance spectrum showed a band edge around 255 nm Strong absorption band in the UV-light region is noticed, and the corresponding band gap observed to be 3.98 eV for 1wt% Co/MS, which is gradually decreased as the concentration of material increased, i.e., 3.69eV for 20wt% which is seen in Fig. 2(b).

A crucial component of catalytic activity is the produced materials' optical absorption wavelength. The catalyst's photocatalytic activity will be maximal when enough electrons are stimulated from the valence band to the conduction band. The catalyst that is supplying incident light energy is equal to or greater than the band gap energy of the photocatalyst. Fig. 2(b) depicts the results of the Tauc plot. Using the Tauc equation, (hν) 1/n= A(h Eg), the energy band gap was calculated. The extrapolation in the linear region of the plot gives an energy band gap, Eg.

Where,

α is the absorption coefficient

h is Planck's constant

ν is the vibration frequency

n is a sample transition, and

'A' is a proportionality constant

The results of the UV-visible absorption demonstrated that the mixed oxide nanomaterials are capable of producing more electrons and holes when exposed to UV light. The holes and electrons produced during catalytic reactions will actively take part in the oxidation and reduction process. These findings revealed that the Co/MS nanomaterial had a greater photocatalytic efficiency.

X-Ray Diffraction Analysis

The prepared Co/MS nanostructures were subjected to X-ray analysis in order to identify the phase and crystalline size of nanomaterials; various amounts of (1, 5, 10,15, and 20 wt.%) Co-doped on MoO_3 supported on SiO_2 were investigated by X-ray diffraction studies over the 2θ values in the range of 10-80°. The intense XRD peaks confirm the formation of highly crystalline materials with mainly two phases, i.e., α-MoO_3 and $CoMoO_4$ (Fig. 3).

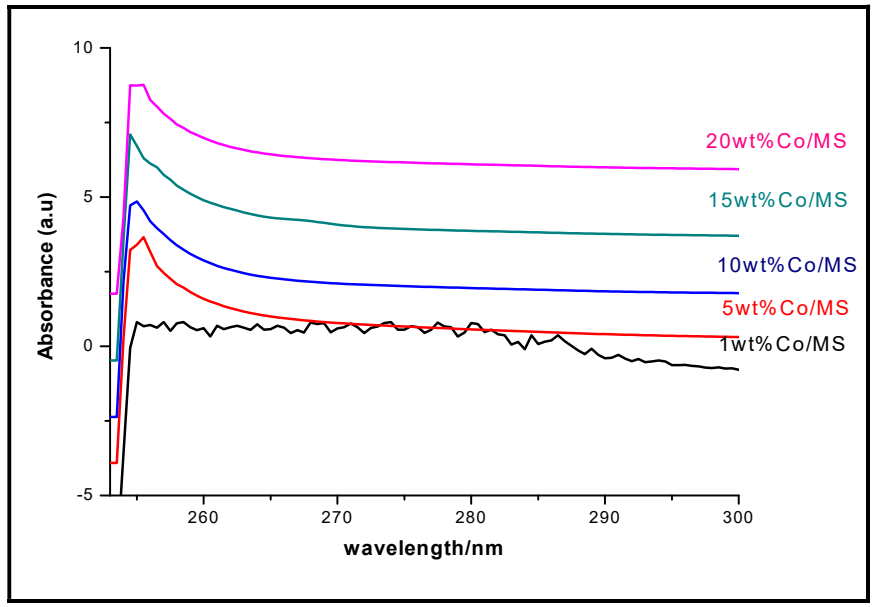

Fig. 2(a): UV Spectra of 1-20wt% Co/MS nanomaterials.

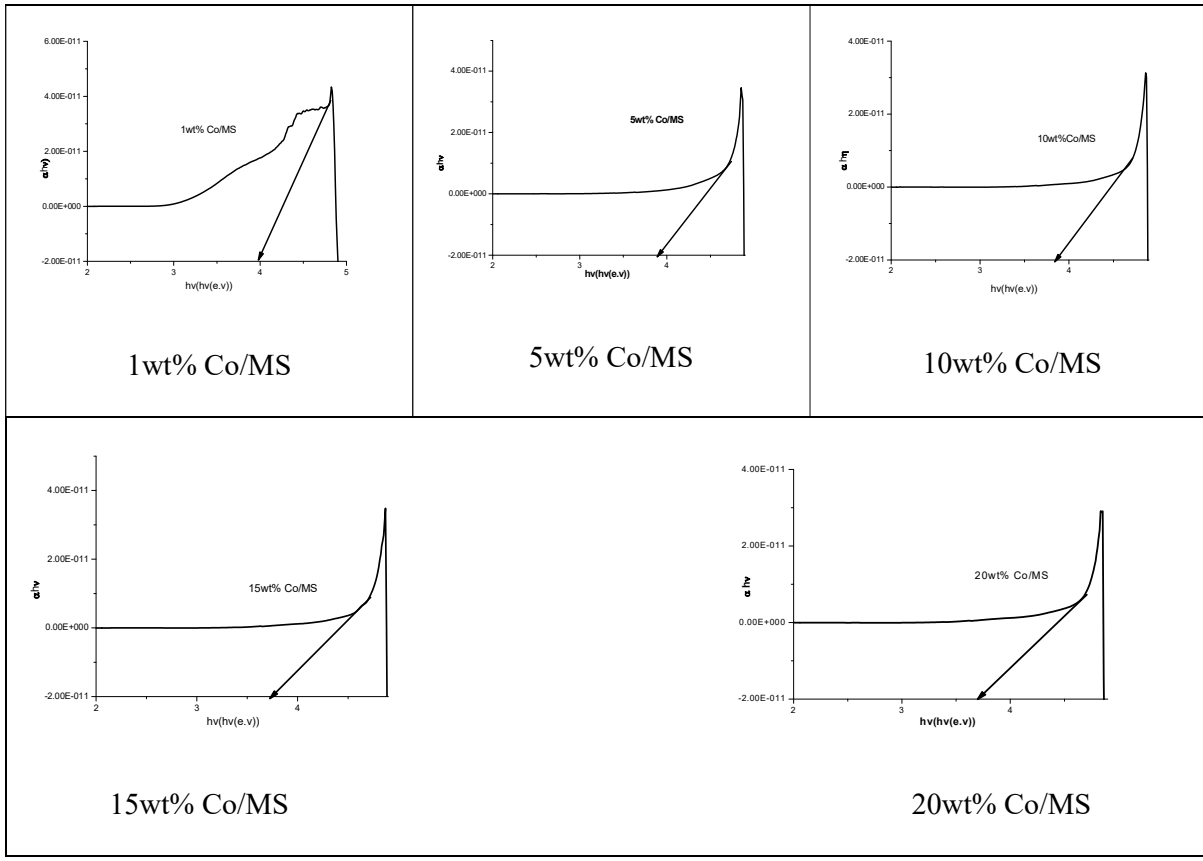

Fig. 2(b): Band gap graph for 1-20wt% Co/MS.

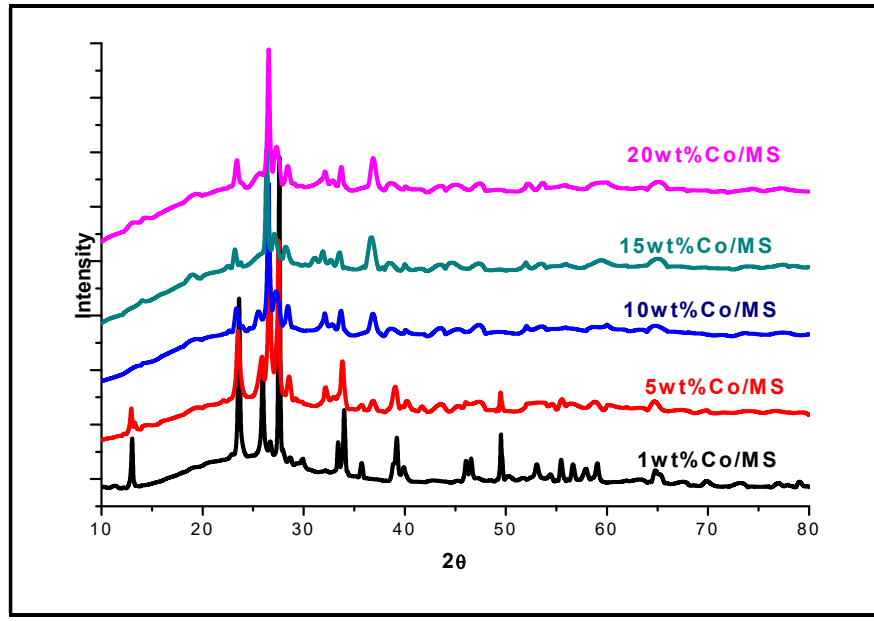

Fig. 3: XRD Spectra of Co/Mo/SiO_2 nanomaterials.

The diffraction peak for α-MoO_3 can be assigned to 12.98°, 25.87°, 27.51°, 33.86°, 35.67° and 49.52° indexed as (020), (040), (021), (111), (041) and (002). $CoMoO_4$ indicated 2θ at 23.44°, 27.61°, 28.46°, 45.75° and 59.43° indexed as (021), (22-1), (220), (420) and (35-1). Which exactly matches with (JCPDS NO-01-073-6497) and (JCPDS NO-00-25-1434), respectively. The crystallite size in the range of 10 nm to 70 nm was calculated from the Debye Scherrer equation ($D=0.9\lambda/\beta \cos\theta$), where

D is the crystal size

λ is the wavelength of X-ray

θ is the Braggs angle in radians and

β is the full width at half maximum of the peak in radians

SEM and EDX Analysis

Based on SEM images that were captured, the surface morphology of the as-prepared samples was examined, and an EDX analysis of the created nanomaterials was done, and the results are shown in Fig. 4 (a, b, c, d, and e). In 1-20wt% Co/MS showed global and uniform particles with spherical shapes that are coherent together.

Using energy dispersive X-ray spectroscopy analysis, the chemical makeup of samples 1 and 20 wt% Co/MS oxide particle was examined. The spectra are displayed in Fig. 5(a) and 5(b), with the peaks indicating the components present in the samples. The representative EDX data in Fig. 5(a) and 5(b) shows two intense and prominent peaks of molybdenum and silica and other comparatively smaller peaks of cobalt. These results confirmed the existence of Co atoms in the nanomaterials. Consequently, it may be concluded that Co ions are evenly distributed throughout the molybdenum and silica oxide crystallites.

Photodegradation Studies

The effect of the presence of the nanomaterials on the photodegradation of MO dye was evaluated under visible light irradiation. For the degradation, a 100 mL solution containing 10 ppm methyl orange (MO) dye was chosen for the study of the photocatalytic activity of prepared samples. The 1-liter stock solution of 10 ppm dyes was prepared by dissolving 10 mg of MO in deionized water. For the evaluation of photocatalytic activity, 100 mL, 10 ppm of each dye solution was taken in a 250 mL conical flask. About 100mg of Co/Mo/SiO_2 nanomaterials was added.

This reaction was carried out in a closed box fitted with the lamp was 200W, and the distance between the lamp and the reaction mixture was fixed throughout the study (10 cm). Before being exposed to light, the suspension was agitated for 30 min in the dark to create equilibrium between the catalyst and substrate. Subsequently, the suspension was continuously stirred while exposed to visible light. At various intervals during the irradiation process, 2 mL of the suspension was routinely removed from the reactor. For MO in aqueous heterogeneous solution suspensions, the absorption peak at 470 nm was used to quantitatively assess the catalyst's catalytic activity. The % of dye degradation was computed using the following formula.

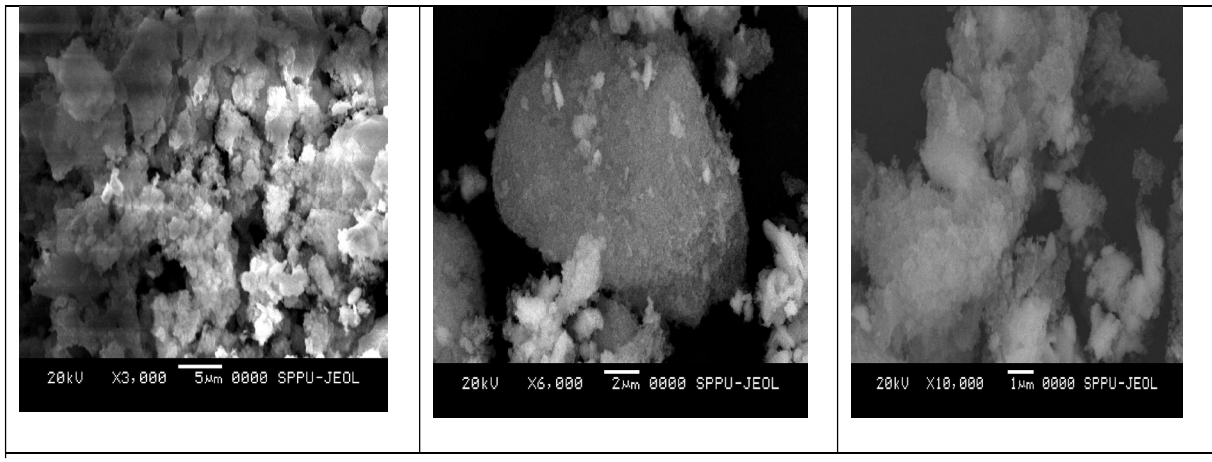

Fig. 4(a). 1wt% Co/MS.

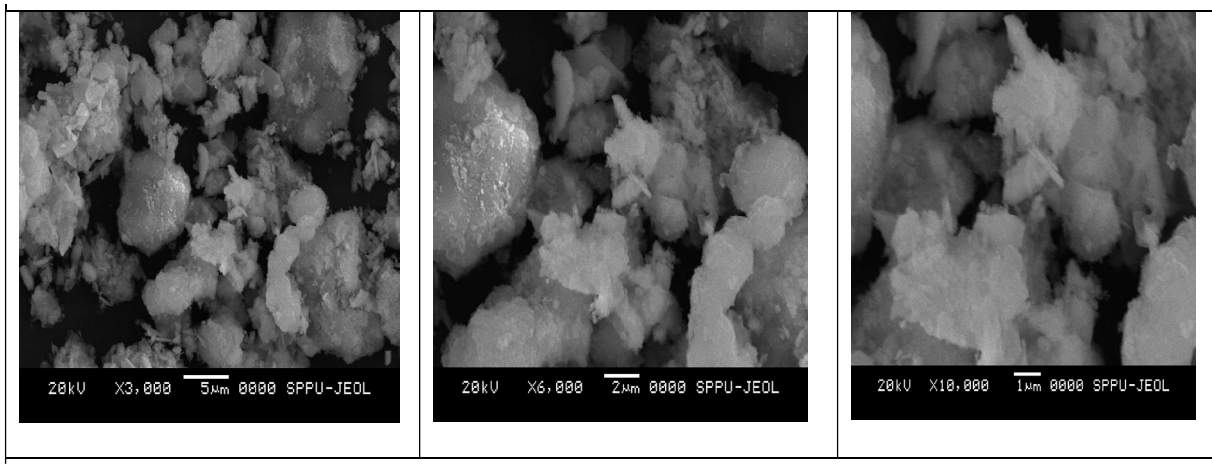

Fig. 4(b): 5wt% Co/MS.

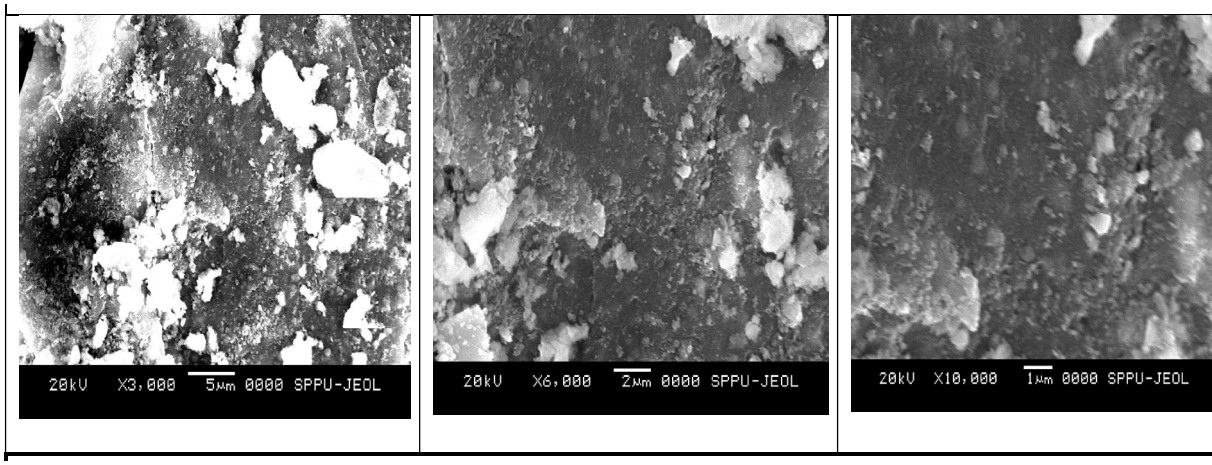

Fig. 4(c): 10wt% Co/MS.

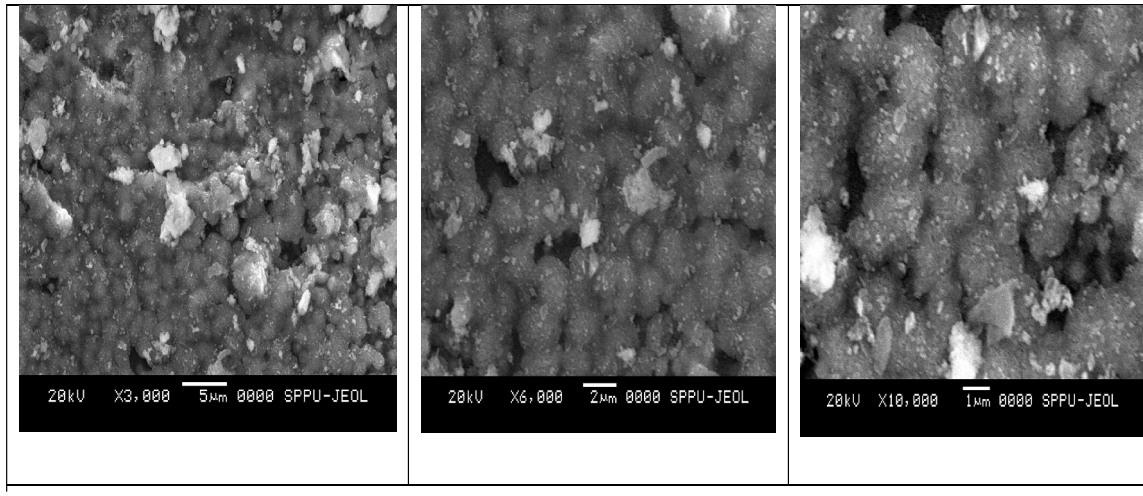

Fig. 4(d): 15wt% Co/MS.

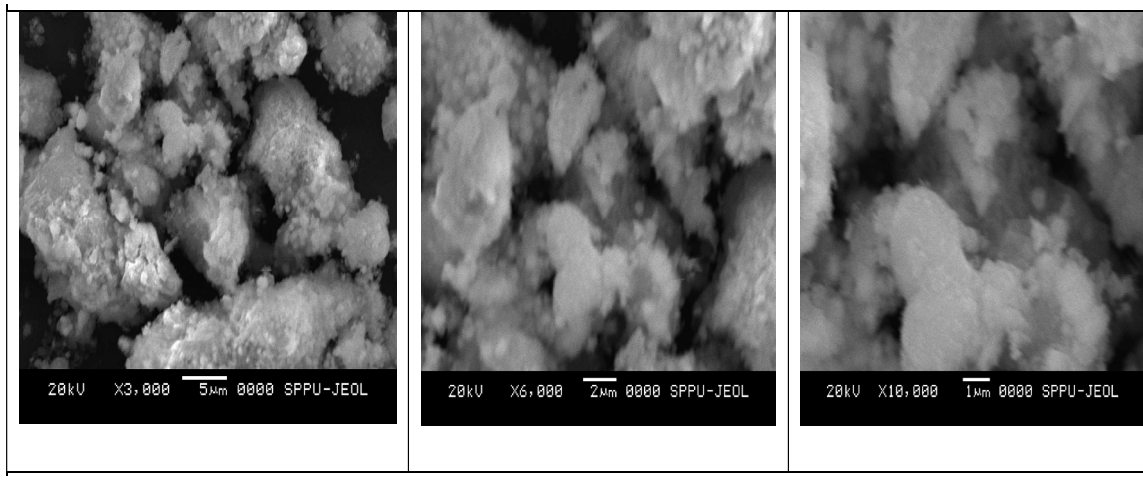

Fig. 4(e): 20wt% Co/MS.

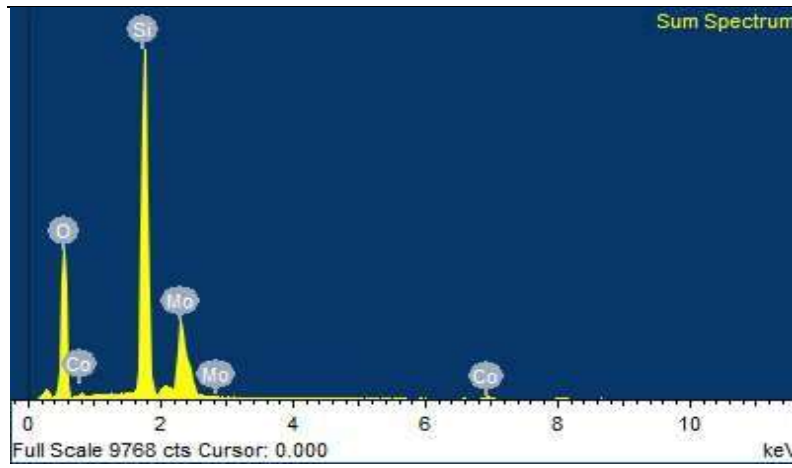

Fig. 5(a): EDX graph of 1wt% Co/MS.

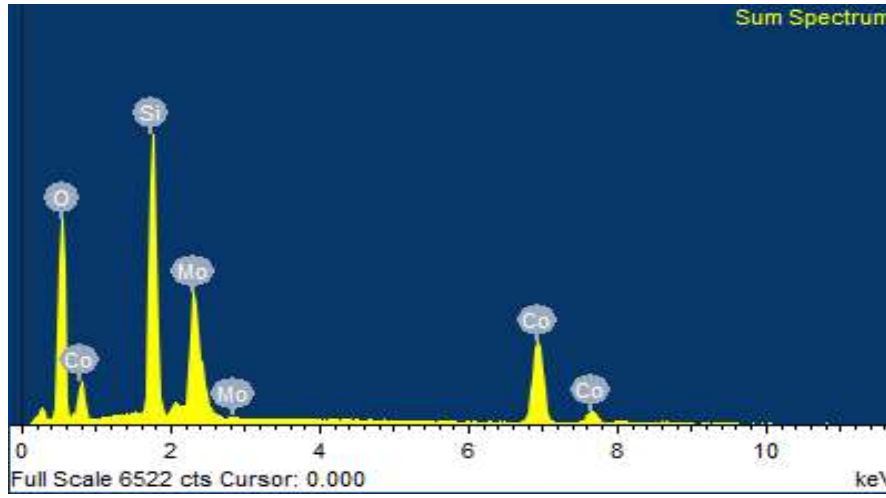

Fig. 5(b): EDX graph of 20wt% Co/MS.

Degradation Efficiency = {(C0-Ct)/C0 × 100 …(1)

Where C0 is the initial concentration of the dye solution,

Ct is the concentration of the dye solution after photoirradiation in a selected time interval.

Photodegradation of Cobalt Doped MS Nanostructures

Following thorough structural and optical characterization, the degradation of MO dye under a 200W lamp was used to assess the photocatalytic activity of the 1, 5, 10, 15, and 20wt% Co/MS nanomaterials. The step-by-step instructions are listed below. The main purpose of stirring the solution in the dark was to monitor the adsorption-desorption equilibrium. The MO solution sample was taken out of the reaction mixture at prearranged intervals, and its absorption spectra were recorded to track the rate of degradation and removal effectiveness. Fig. 6 shows the representative absorption spectra of MO solution following the degradation experiment in the presence of 1–20% Co/MS samples. After 180 minutes of irradiation, it was evident that the absorption peak of the MO solution isolated from the 20wt% sample (Fig. 6(e)) had a greater reduction in peak intensity. Thereby indicating its superior dye-removal efficiency compared to the other four samples (Fig. 6 (a-d)).

More precisely, 38.50%, 54.15%, 56.84%, 61.94%, and 71.23% of MO dye was degraded by 1wt%, 5wt%, 10wt%, 15wt% and 20wt% Co/MS samples, respectively (Fig. 6 d).

The presence of larger cobalt concentrations in the host lattice-possibly because of a lower band gap energy-can be the reason for the 20wt% sample's improved photocatalytic performance when compared to the 1–15wt% sample.

Degradation Mechanism

Because of its lower bandgap, the Co/MS sample absorbs UV-visible radiation from solar radiation, which causes its valence electrons to move from the valence band (VB) to the conductive band (CB). The valence electron was excited, resulting in the creation of a positively charged (h+) hole in the VB. By acting as a trapping agent for the excited electrons, the Co/MS sample decreased the likelihood of electron-hole recombination (Fig. 7). Acting as an intermediary, the Co and Mo contents first captured excited electrons, which they then utilized to convert molecular oxygen (O_2) into the superoxide radical O_2 (free radical). After being excited by electrons, the positively charged hole (h+) created in the VB further interacted with H_2O or OH to form the hydroxyl free radical OH^-.

Thus, in brief, molecular oxygen and water were transformed into secondary active free radicals (O_2/OH) via oxidation/reduction reactions involving the primary active species, free electrons, and holes. Ultimately, the organic MO dye was broken down into straightforward, non-toxic metabolites by the highly active free radicals' interaction with it. The following diagram summarizes the mechanism of the entire degradation process.

Antibacterial Activity

The antibacterial activity of all compositions (1wt%, 5wt%,10wt%,15wt%, and 20wt%) of Co/MS samples against Gram-positive (*Bacillus subtilis, Staphylococcus aureus*), Gram-negative (*Escherichia coli, Klebsiella pneumoniae*) and fungal *(Aspergillus niger, Candida albicans*) was examined by using well diffusion method as shown in

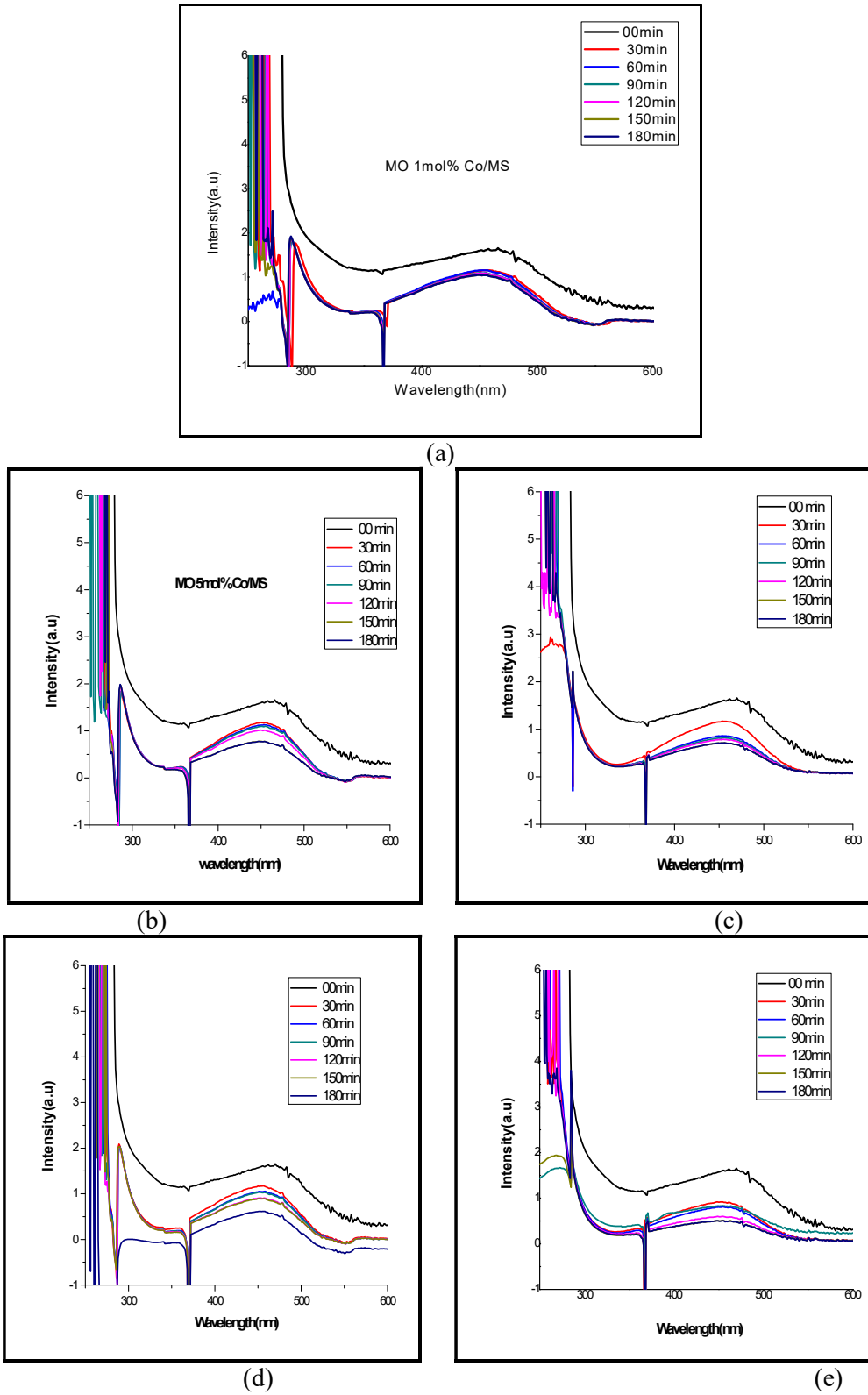

Fig. 6: Absorption spectra for the degradation of MO dye over (a) 1wt%, (b) 5wt%, (c) 10wt%, (d) 15wt% and (e) 20wt%Co/MS.

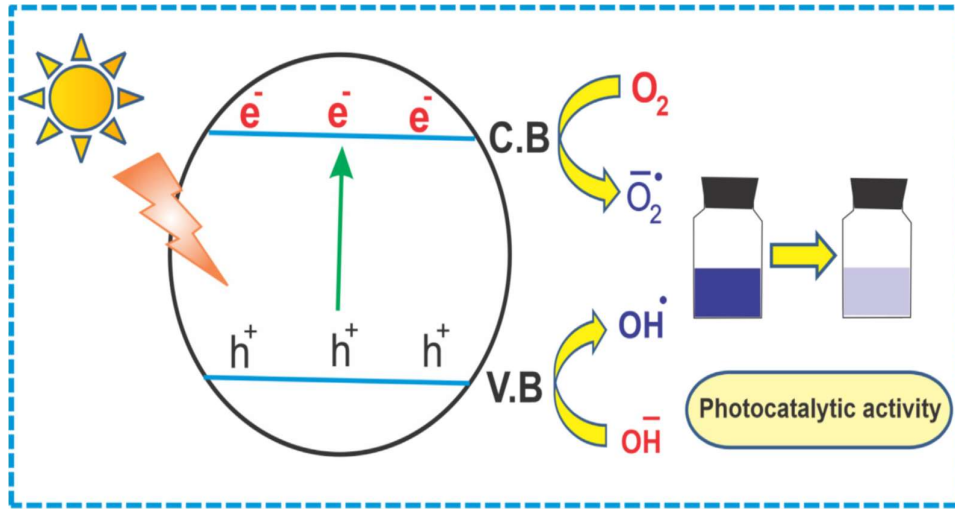

Fig. 7: Mechanism of the degradation process (Zhang et al. 2010).

Fig. 8(a): Antimicrobial activity of Co/MS catalyst against *Staphylococcus aureus*.

Fig. 8(b): Antimicrobial activity of Co/MS catalyst against *Bacillus subtilis*.

Fig. 8(c): Antimicrobial activity of Co/MS catalyst against *E. coli*.

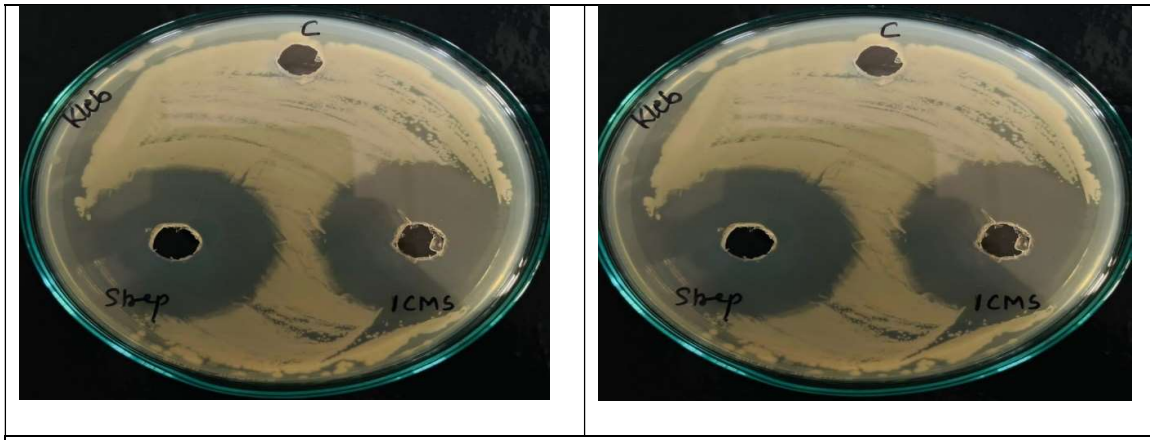

Fig. 8(d): Antimicrobial activity of Co/MS catalyst against *Klebsiella pneumonia*.

Table 1(a): Zone of inhibition in mm for Co/MS materials for microbial strains.

Catalyst %	Zone of inhibition in mm			
	S. aureus	B. subtilis	E.coli	K.pneumoniae
1wt% Co/MS	27 ± 0.02	23 ± 0.02	21 ± 0.01	27 ± 0.02
5wt% Co/MS	28 ± 0.03	24 ± 0.01	22 ± 0.02	28 ± 0.03
10wt% Co/MS	32 ± 0.02	27 ± 0.02	20 ± 0.04	32 ± 0.02
15wt% Co/MS	33 ± 0.01	28 ± 0.03	18 ± 0.01	33 ± 0.01
20wt% Co/MS	35 ± 0.02	32 ± 0.02	22 ± 0.02	35 ± 0.02
Std. Streptomycin	23 ± 0.02	22 ± 0.02	19 ± 0.01	23 ± 0.02
Control (DMSO)	00	00	00	00

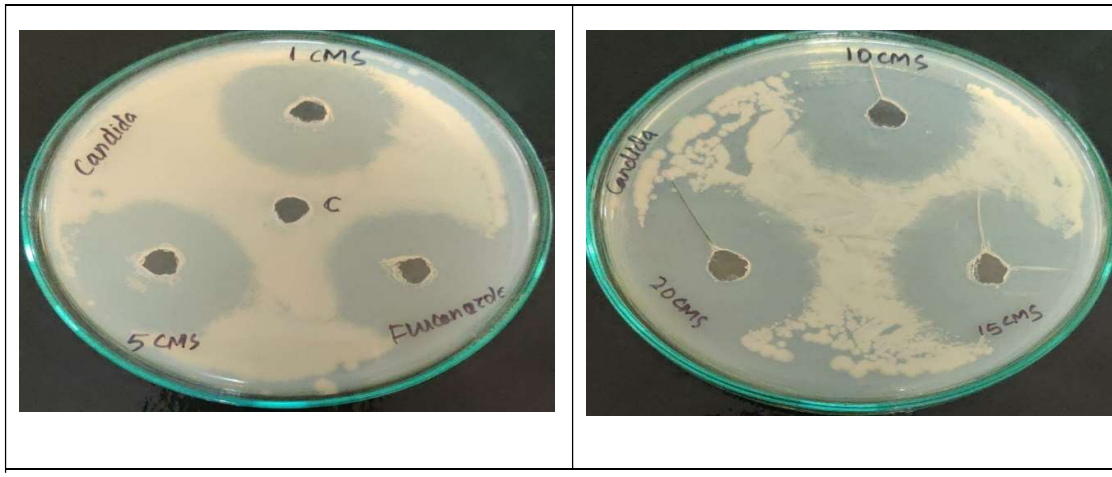

Fig. 9(a): Antimicrobial activity of Co/MS catalyst against *Candida albicans*.

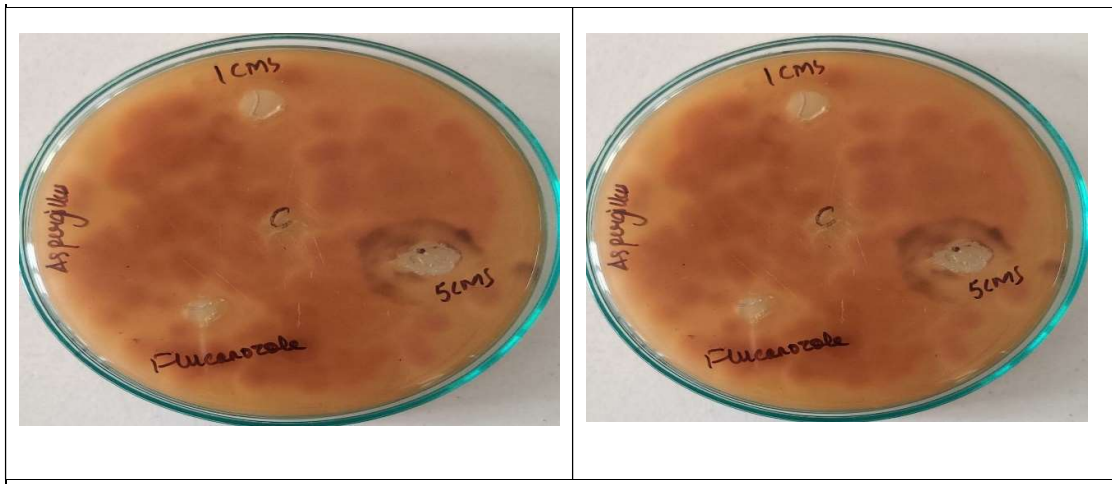

Fig. 9(b): Antimicrobial activity of Co/MS catalyst against *Aspergillus niger.*

Table 1(b): Zone of inhibition in mm for Co/MS materials for fungal strains.

Catalyst %	*Candida albicans*	*Aspergillus niger*
1wt% Co/MS	21 ± 0.02	05 ± 0.01
5wt% Co/MS	24 ± 0.03	10 ± 0.03
10wt% Co/MS	27 ± 0.03	09 ± 0.03
15wt% Co/MS	29 ± 0.01	08 ± 0.02
20wt% Co/MS	32 ± 0.02	10 ± 0.01
Std. Flucanozole	22 ± 0.02	01 ± 0.03
Control (DMSO)	00	00

Figs. 8(a-d) and 9(a and b), all prepared samples illustrated good antibacterial activity against both Gram-positive and Gram-negative bacterial and fungal strains, respectively. Table 1(a and b) summarises the comparative results of measuring inhibition areas in all samples.

It is evident from the antibacterial results that the 20wt% Co/MS sample exhibited a superior antibacterial aptitude than that of a 1-15% Co/MS and standard against Gram-positive and Gram-negative bacteria as well as fungal strains. There was a continuous increase in the inhibition zone as the concentration of Co/MS catalysts increased from 1wt%–20wt%. 20wt% concentrations are more crystalline, which is the reason they have shown more inhibition of microorganisms because the activity of Co/MS catalysts depended on the size and structure responsible for the inhibition of microbe. Nanomaterial incorporation inhibits phagocytosis, inhibits oxidative stress, limits cell development, lowers cell viability, and eventually compromises cell integrity. The production of reactive oxygen species (ROS), which can harm cellular proteins, lipids, and the cell wall membrane and ultimately destroy the bacteria's cell, is one of the crucial steps in increasing toxicity.

The antifungal activities of Co/MS catalysts are carried out towards two fungal strains, *Candida albicans,* and *Aspergillus niger,* and their activity was referred to standard antifungal agent fluconazole. The results are brief in Tables 1(a) and 1(b). Among the two fungus species, *Candida albicans* and *Aspergillus niger* have been observed with good antifungal effects. From Table 1(b), it is seen that *Candida albicans* showed more antifungal activity than *Aspergillus niger* for all Co/MS catalysts.

CONCLUSION

The cobalt-doped molybdenum-supported silica oxide nanocatalysts were synthesized by the Sol-gel method. The powder X-ray diffraction analysis confirmed the good crystalline nature. The presence of functional groups was established by FTIR analysis. Results of the UV-Vis spectrum indirect transition band gap shifted from Eg = 3.98 eV to 3.69 eV. SEM-EDX data showed that all materials in Co/MS were agglomerated with spherical shape and materials were prepared in good composition. A photodegradation study of MO dye stated that 20wt% Co/MS gave higher degradation efficiency for methyl orange dye as compared to 1-15 wt% Co/MS. From the antibacterial and antifungal study, it is concluded that 20% Co/MS nanocatalyst showed the highest zone of inhibition for both microbial as well as fungal species, and nanocomposite material is suitable for antibiotic applications.

REFERENCES

Bian, Z., Cao, F., Zhu, J. and Li, H., 2015. Plant uptake-assisted round-the-clock photocatalysis for complete purification of aquaculture wastewater using sunlight. *Environmental Science & Technology*, 49, pp.2418.

Buonomenna, M., 2013. Membrane processes for a sustainable industrial growth. *RSC Advances*, 3, pp.5694.

Chiang, T.H. and Yeh, H.C., 2014. A novel synthesis of -MoO3 nanobelts and the characterization. *Journal of Alloys and Compounds*, 585, pp.535–541.

Dong, W. and Dunn, B., 1998. Sol-gel synthesis of monolithic molybdenum oxide aerogels and xerogels. *Journal of Materials Chemistry*, 8, pp.665–670.

Fang, G., Wu, Y., Dong, X., Liu, C., He, S. and Wang, S., 2013. Synthesis, characterization, and photocatalytic activity of tungsten oxide nanostructures. *Journal of Agricultural and Food Chemistry*, 61, pp.3834.

Gita, S., Hussan, A. and Choudhury, T.G., 2017. Impact of textile dyes waste on aquatic environments and its treatment. *Environment & Ecology*, 35(3C), pp.2349-2353.

Hawkey, P.M., 2008. The growing burden of antimicrobial resistance. *Journal of Antimicrobial Chemotherapy*, 62(Suppl 1), pp.1–9.

Isik, M. and Sponza, D.T., 2005. Characterization of sulfate-reducing bacteria anaerobic granular sludge and granulometric analysis with grey relation. *Bioresource Technology*, 96, pp.633.

Jones, N., Ray, B., Ranjit, K.T. and Manna, A.C., 2008. Antibacterial activity of ZnO nanoparticles suspensions on a broad spectrum of microorganisms. *FEMS Microbiology Letters*, 279, pp.71–76.

Kant, R., 2015. Textile dyeing industry an environmental hazard. *Natural Science*, 4(1), Article ID:17027, pp.5.

Komolafe, O.O., 2003. Antibiotic resistance in bacteria – an emerging public health problem. *Malawi Medical Journal*, 15, pp.63–67.

Kou, J., Zhou, X., Lu, H., Wu, F. and Fan, J., 2014. The effect of temperature on water desalination through two-dimensional nanopores. *Nanoscale*, 6, pp.1865.

Lan, S., Liu, L., Li, R., Leng, Z. and Gan, S., 2014. Preparation of ZnO photocatalyst for the efficient and rapid photocatalytic degradation of azo dyes. *Industrial & Engineering Chemistry Research*, 53, pp.3131.

Lellis, C., Zani, F. and João, A.P., 2019. Effects of textile dyes on health and the environment and bioremediation potential of living organisms. *Biotechnology Research and Innovation*, 3(2), pp.275-290.

Lu, J., Zhang, P., Li, A., Su, F., Wang, T., Liu, Y. and Gong, J., 2013. Mesoporous N-doped TiO2 with enhanced adsorption and visible light photocatalytic activity. *Chemical Communications*, 49, pp.5817.

Manzoor, J. and Sharma, M., 2020. *Impact Of Textile Dyes on Human Health and Environment*. IGI Global Publishing

Mills, A., Davies, R. and Worsley, D., 1993. Water purification by semiconductor photocatalysis. *Journal of the Chemical Society, Reviews*, 22, pp.417.

Muhammad, A., Rahman, A., Zulfiqar, S., Alsafari, I.A. and Shahid, M., 2021. Facile synthesis of binary metal substituted copper oxide as a solar light-driven photocatalyst and antibacterial substitute. *Advanced Powder Technology*, 32, pp.940–950.

Pandit, V.U., Ambekar, J., Arbuj, S.S. and Rane, S.B., 2015. Synthesis of hierarchical ZnO nanostructure and its photocatalytic performance study. *Journal of Nanoengineering and Nanomanufacturing*, 5, pp.1-5.

Putatunda, S., Sen, D. and Bhattacharjee, C., 2015. Microbial production of phenol via salicylate decarboxylation. *RSC Advances*, 5, pp.52676.

Rahman, R., Samanta, D., Pathak, A. and Nath, T.K., 2021. Tuning of structural and optical properties with enhanced catalytic activity in chemically synthesized Co-doped MoS2 nanosheets. *RSC Advances*, 11, pp.1303.

Weber, H. and Sciubba, J.D., 2019. The effect of population growth on the environment: evidence from European regions. *European Journal of Population*, 35(2), pp.379–402.

Zhang, Y., Singh, S. and Bakshi, B., 2010. Accounting for ecosystem services in life cycle assessment, Part I: A critical review. *Environmental Science & Technology*, 44, pp.2232.

ORCID DETAILS OF THE AUTHORS

S. R. Gadale: https://orcid.org/0000-0002-2872-505X